




# Synthesis and characterization of Ti-doped $\text{ZrSiO}_4$ at ambient and high-pressure conditions

S. Ferrari<sup>1,\*</sup> , F. Grinblat<sup>1</sup>, V. Bilovol<sup>1</sup>, L. G. Pampillo<sup>1</sup>, F. D. Saccone<sup>2</sup>, D. Errandonea<sup>3</sup>, and C. M. Chanquía<sup>4</sup>

<sup>1</sup> Consejo Nacional de Investigaciones Científicas y Técnicas, Instituto de Tecnología y Ciencias de la Ingeniería "Ing. Hilario Fernández Long" (INTECIN), Universidad de Buenos Aires, Av. Paseo Colón 850, C1063ACV Buenos Aires, Argentina

<sup>2</sup> Departamento de Física, Facultad de Ingeniería, Universidad de Buenos Aires, Av. Paseo Colón 850, C1063ACV Buenos Aires, Argentina

<sup>3</sup> Departamento de Física Aplicada, Institut Universitari de Ciència dels Materials, Universitat de Valencia, c/Doctor Moliner 50, Burjassot, 46100 Valencia, Spain

<sup>4</sup> Centro Atómico Bariloche, Comisión Nacional de Energía Atómica (CAB-CNEA), Av. Bustillo 9500, R8402AGP Bariloche, Río Negro, Argentina

Received: 24 November 2017

Accepted: 23 February 2018

© Springer Science+Business Media, LLC, part of Springer Nature 2018

## ABSTRACT

We have successfully synthesized for the first time a Ti-doped  $\text{ZrSiO}_4$  powder (stoichiometry  $\text{Zr}_{0.95}\text{Ti}_{0.05}\text{SiO}_4$ ) via a sol–gel route. The structural and vibrational properties have been characterized by X-ray diffraction, electron microscopy and Raman spectroscopy.  $\text{Zr}_{0.95}\text{Ti}_{0.05}\text{SiO}_4$  has a tetragonal zircon-type structure with  $a = 6.5981(2)$  Å and  $c = 5.9810(2)$  Å. Eight of its Raman-active modes have been measured and assigned. We also performed high-pressure synchrotron X-ray diffraction experiments. The structural behavior was studied up to 31 GPa. At this pressure, we found evidence of the onset of a phase transition, coexisting the low-pressure polymorphs (zircon) with the typical high-pressure polymorph of  $\text{ZrSiO}_4$  (reidite-type). From the analysis of unit-cell volume versus pressure using a Birch–Murnaghan equation of state, in the quasi-hydrostatic pressure regime ( $P < 10.5$  GPa), we have determined a bulk modulus of 297 GPa. This magnitude represents an enhancement of a 30% in the value of this parameter if compared with un-doped zircon-type  $\text{ZrSiO}_4$  (bulk modulus  $< 227$  GPa). The low compressibility of  $\text{Zr}_{0.95}\text{Ti}_{0.05}\text{SiO}_4$  converts this compound in a very good candidate for many technological applications. The effect of pressure on the linear compressibility of the lattice parameters is also analyzed.

Address correspondence to E-mail: sferrari@fi.uba.ar

## Introduction

The development of new materials added to the interest of their properties under extreme conditions is some of the reasons that promote the investigation in the area of high-pressure (HP) research. The addition of a doping element to a material can change the behavior of the structural and elastic properties under compression as well as modifying the transition pressure and structural sequence. Such phenomena have been observed, for instance, in Fe-doped SnO<sub>2</sub> nanoparticles [1]. Another of the goals of HP research is to produce ultra-hard and ultra-incompressible materials [2], for example cubic boron nitride. In particular, theoretical studies have predicted that zircon-type TiSiO<sub>4</sub> [3–5] could be an ultra-hard material with a bulk modulus larger than in ZrSiO<sub>4</sub>. This converts TiSiO<sub>4</sub> in a good candidate for many technological applications. However, to the best of knowledge, up to date, nobody has succeeded in synthesizing crystalline TiSiO<sub>4</sub> and therefore the theoretical prediction has not been confirmed.

Due to the fact that it has not been yet possible to synthesize crystalline TiSiO<sub>4</sub>, an alternative approach to experimentally explore the foreseen incompressibility of this silicate is to study the mechanical properties of Ti-doped zircon-type ZrSiO<sub>4</sub>. This will allow to infer if the substitution of Zr for Ti increases the incompressibility of the material. Following this reasoning, in this work we prepared by the first time Ti-doped ZrSiO<sub>4</sub> (Zr<sub>0.95</sub>Ti<sub>0.05</sub>SiO<sub>4</sub>) by the partial substitution of Zr by Ti in a ZrSiO<sub>4</sub> (zircon) sol-gel chemical route. The preparation of such compound has an additional interest because titanium-rich silicates have received attention due to their high activity as photocatalytic materials and their optical properties [6]. In addition, theoretical studies have suggested that doping zircon with Ti reduces the electronic band gap, making it more useful as a phosphor material [7]. On the other hand, Ti-doped zircon-type oxides are found in Earth mantle-sourced kimberlites, being thus the knowledge of their compressibility of relevance for studying the asthenosphere and subcontinental lithospheric mantle [8].

The compressibility of zircon-type ZrSiO<sub>4</sub> has been widely studied [9–14]. It is known that this silicate undergoes a phase transition to the scheelite-type structure at ~ 19.7 GPa [14]. The HP polymorphs is known as reidite. Zircon-type USiO<sub>4</sub>, HfSiO<sub>4</sub> and

ThGeO<sub>4</sub> undergo the same phase transition at 17.0, 19.6 and 12.3 GPa, respectively [11, 15, 16]. In addition, all the zircon-type oxides are known to have a similar bulk modulus, determined mainly by compressibility of the Zr–O (or equivalent) bonds [15]. However, compressibility can be affected by the incorporation of impurities as proposed based upon studies on synthetic and natural ZrSiO<sub>4</sub> [14]. Nevertheless, until now there are no systematic studies on the influence of the incorporation of impurities on the compressibility of ZrSiO<sub>4</sub>. The present study of Zr<sub>0.95</sub>Ti<sub>0.05</sub>SiO<sub>4</sub> will contribute to understand the influence of impurities in the mechanical properties and structural stability of ZrSiO<sub>4</sub>. In order to do it, we have analyzed the results of X-ray diffraction (XRD) data taken in situ under high-pressure conditions on Zr<sub>0.95</sub>Ti<sub>0.05</sub>SiO<sub>4</sub>. The measurements were carried out in the X-ray diffraction and spectroscopy beamline (better known by its acronym: XDS) at Laboratório Nacional de Luz Sincrotron (LNLS), Campinas, Brazil. The volumetric and axial compressibility were determined from the experiments. In addition, a detailed characterization of the ambient-pressure properties of Zr<sub>0.95</sub>Ti<sub>0.05</sub>SiO<sub>4</sub> is also reported.

## Experimental

Zr<sub>0.95</sub>Ti<sub>0.05</sub>SiO<sub>4</sub> was synthesized via a sol-gel route based on the procedure described by Veytizou et al. [17, 18]. The sample was prepared using starting high-purity precursors (Alfa Aesar): tetraethoxysilane (TEOS), titanium(IV) isopropoxide (TIP) and hydrated zirconyl nitrate. In a typical procedure, hydrated zirconyl nitrate was dissolved in ultra-pure water and TEOS was added in a stoichiometric ratio with mixing speed around 300 rpm. On the other hand, TIP was dissolved in ultra-pure water inside a nitrogen-filled glove box (oxygen and moisture concentrations < 4 ppm), and then it was added to the first solution. When the precursor solution became clear, it was treated under reflux at 100 °C for 24 h. Subsequently, this solution was added to a dilute aqueous ammonia solution (~ 1 vol%) with a stirring speed around 200 rpm. A colloidal precipitate was immediately formed which was filtered and washed several times with ultra-pure water to obtain pH ~ 7. This precipitate was dried overnight at 100 °C in a muffle and subsequently was grinded with an agate mortar. The precursor powder was

thermally treated at 1500 °C during 6 h in air atmosphere (heating/cooling ramps of 5 °C/min). Finally, for comparative purpose, un-doped ZrSiO<sub>4</sub> was also synthesized by the same procedure (without Ti addition).

The obtained powders were characterized by X-Ray diffraction (XRD), scanning-electron microscopy (SEM), energy-dispersive X-ray spectroscopy (EDS), Raman spectroscopy and high-pressure XRD (HP-XRD) at room temperature. Ambient-pressure XRD was carried out with a Rigaku D/max diffractometer equipped with a vertical goniometer, using a Bragg–Brentano geometry ( $\theta$ – $2\theta$  coupled arms) and Cu-K $\alpha$  radiation in the  $20^\circ \leq 2\theta \leq 80^\circ$  range, measuring at every 0.03° step and sweeping with a 1° per minute velocity. The SEM micrographs were taken using a FEI QUANTA 200 microscope, equipped with an X-ray spectrometer for EDS measurements. The Raman signal of the powder samples was recorded using a NRS-4100 micro-spectrometer (JASCO) with a focal length of 200 mm, equipped with a 900 l/mm grating and an edge filter. The excitation beam was provided by a green (Nd:YAG) laser at 532.34 nm. The laser power was 20 mW (resulting in ~ 8.1 mW at sample). The laser was vertically polarized and coupled on a microscope system to focus the laser on the sample using a 20X achromat objective (RMS20X—Olympus) collecting the Raman signal in the backscattering configuration. The laser spot size was of about 1.6  $\mu\text{m}$  in diameter and the slit aperture was 100  $\mu\text{m}$ . The scanning range of interest in wave numbers is 100–1200  $\text{cm}^{-1}$ . A silicon standard was used for the calibration of the Raman system. The acquisition time (5 s) and the number of accumulations (10) were chosen to provide a satisfactory spectrum and to optimize the noise-to-signal ratio. The spectral resolution was better than 1  $\text{cm}^{-1}$ .

HP powder XRD experiments were performed at the XDS beamline of LNLS, Campinas, Brazil. Pressure was applied by means of a membrane diamond-anvil cell (DAC), with a gasket pre-indented to a thickness of 60  $\mu\text{m}$ . The DAC was equipped with diamond-anvils with a culet diameter of 300  $\mu\text{m}$ . The diameter of the pressure chamber drilled into the gasket was 100  $\mu\text{m}$ . The applied pressure was determined by the ruby fluorescence method with an accuracy of 0.1 GPa [19]. A 4:1 methanol–ethanol mixture, which remains quasi-hydrostatic up to 10.5 GPa, was used as pressure-transmitting medium (PTM) [20]. Special caution was taking during sample

loading into the DAC to avoid sample bridging under compression [21, 22]. The experiments were performed in the angle-dispersive configuration with a monochromatic beam with 110  $\mu\text{m}$  width and a wavelength of 0.6199 Å. The images were collected using a charge-coupled device detector (Rayonix 165). The structural analysis was performed using MAUD [23].

## Results

### SEM and EDS

EDS analysis was employed to confirm the chemical composition and purity of the prepared Ti-doped ZrSiO<sub>4</sub> sample. The composition found was 0.8 at.% Ti, 15.8 at.% Zr, 16.6 at.% Si and 66.6 at.% O. These results are in an excellent agreement with the nominal composition of the sample. The presence of impurities was not detectable within the accuracy of the instrument. Figure 1 shows the morphology and size of the synthesized material. As clearly evidenced from the electron micrographs, the raw powder has a uniform morphology, being mainly constituted of micron-size quasi-spherical particles. Most of them have a diameter smaller than 5  $\mu\text{m}$ . There are also smaller particles, which appear as bright white particles in the micrograph. Their analysis indicates that they also belong to the same material (Ti-doped ZrSiO<sub>4</sub>). Because of our study was oriented to analyze

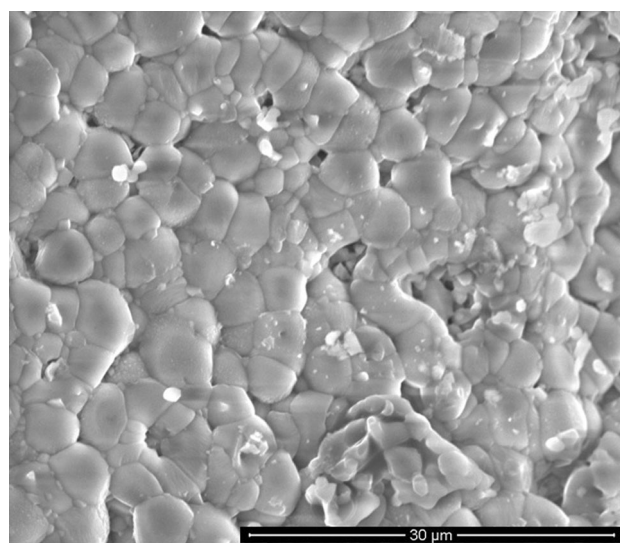


**Figure 1** SEM micrograph showing morphology of the Zr<sub>0.95</sub>-Ti<sub>0.05</sub>SiO<sub>4</sub> powder.

the properties and the behavior of Ti-doped  $\text{ZrSiO}_4$  under pressure, the powder product can be considered as appropriated. A more detailed discussion of the sample morphology is not relevant for our purposes.

### Ambient-pressure X-ray diffraction

Figure 2 shows an ambient-pressure powder XRD pattern of  $\text{Zr}_{0.95}\text{Ti}_{0.05}\text{SiO}_4$  with the corresponding Rietveld refinement. We assumed the atomic positions reported for  $\text{ZrSiO}_4$  [12] (considering that Ti substitutes Zr) and followed the procedure described in Ref. [24]. The Bragg peaks in the XRD pattern belongs mainly to a zircon-type tetragonal structure (space group  $I4_1/amd$ ) with lattice parameters  $a = 6.5982(2)$  Å and  $c = 5.9810(2)$  Å. A small amount of tetragonal t- $\text{ZrO}_2$  (space group  $P4_2/nmc$ ) was also detected. The proportion of the phases present in the sample can be estimated from the relative intensity of the main peaks of t- $\text{ZrO}_2$  and  $\text{ZrSiO}_4$  that do not overlap [25]. The concentration of t- $\text{ZrO}_2$  is less than 4%. Consequently, the Ti composition in  $\text{Zr}_{0.95}\text{Ti}_{0.05}\text{SiO}_4$  can be slightly overestimated due to  $\text{ZrO}_2$  segregation. However, the composition change is small and stays within the accuracy of the EDS system. Such small change will not affect the structural properties of the material. No peaks corresponding to any of the phases of  $\text{TiO}_2$  were found [26]. The same

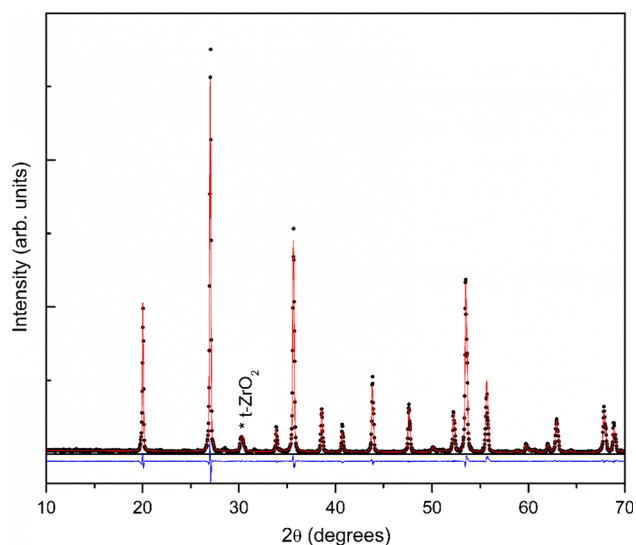


**Figure 2** Experimental XRD pattern (dots) and Rietveld refinement (solid line) at ambient pressure. The trace at the bottom shows the residuals. The star marks the position of the main diffraction peak of t- $\text{ZrO}_2$ .

can be stated for the different phases known for  $\text{SiO}_2$  [27]. The  $R$ -values of the Rietveld refinement are  $R_w$  (%) = 10.6,  $R_p$  (%) = 8.2 and  $R_{\text{exp}}$  (%) = 5.1; while  $\chi^2 = 2.127$ . In Fig. 3a, schematic view of the tetragonal zircon structure of  $\text{ZrSiO}_4$  is shown. The zirconium (titanium) atoms are eight coordinated by oxygen atoms. Silicon is coordinated by four oxygen atoms forming a regular tetrahedron.

We would like to mention here some facts related with the likely incorporation of Ti into  $\text{ZrSiO}_4$ . On the one hand, the introduction of the  $\text{Ti}^{4+}$  ion, into the sol-gel preparation method, favors the formation of a compound with the zircon-type structure, preventing the formation of the cristobalite and monoclinic polymorphs of  $\text{ZrO}_2$  [28]. Previously, the same phenomenon was reported for the introduction of Fe into the preparation of  $\text{ZrSiO}_4$  via the sol-gel method [29]. This is because the metal dopant plays the role of initiator of the zircon-type oxides, favoring the nucleation of the zircon-type structure within the zirconia lattice [30]. On the other hand, when comparing the lattice parameters of the zircon-type phase of  $\text{Zr}_{0.95}\text{Ti}_{0.05}\text{SiO}_4$  with the zircon-type phase synthesized by the same procedure but without titanium addition, we found that the lattice parameter  $a$  is 0.03% shorter in the Ti-doped sample. On the other hand, the lattice parameter  $c$  is 0.03% longer for  $\text{Zr}_{0.95}\text{Ti}_{0.05}\text{SiO}_4$  [for pure  $\text{ZrSiO}_4$ :  $a = 6.6004(1)$  Å and  $c = 5.9829(1)$  Å]. The difference in the lattice parameters among un-doped  $\text{ZrSiO}_4$  and Ti-doped  $\text{ZrSiO}_4$  is larger than the error of the measurements, then unambiguously, the incorporation of Ti modifies the crystalline structure. The unit-cell volume of the un-doped sample is larger than that of the Ti-doped

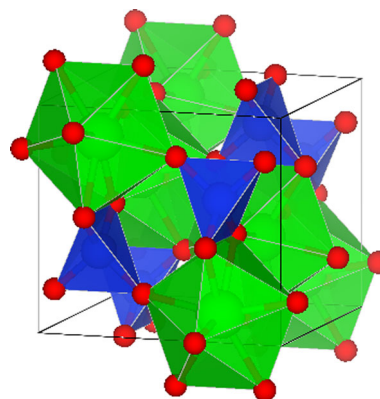


**Figure 3** Schematic view of the tetragonal zircon. The  $\text{SiO}_4$  (blue) and  $\text{ZrO}_8$  (green) polyhedrons are displayed. Ti atoms substitute for Zr atoms.

sample. This is reasonable, given the fact that ionic radius of  $\text{Ti}^{4+}$  is smaller than that of  $\text{Zr}^{4+}$ .

## Raman Spectroscopy

The Raman spectra of  $\text{Zr}_{0.95}\text{Ti}_{0.05}\text{SiO}_4$  and  $\text{ZrSiO}_4$  (the latter prepared in the same way than  $\text{Zr}_{0.95}\text{Ti}_{0.05}\text{SiO}_4$ ) are given in Fig. 4 where the positions of the main peaks are marked. This Raman study was performed with the aim to elucidate how the Ti impurities affect the Raman modes and to compare with previous Raman studies of amorphous  $\text{TiSiO}_4$ . The spectra reveal the known representative peaks from the zircon structure, the most intensive one near  $1000\text{ cm}^{-1}$  [14]. The frequencies of the Raman-active modes are summarized in Table 1 and compared with the literature [31]. The mode frequencies reported in the mentioned table were obtained by fitting the peaks with Lorentzian functions. The agreement with the literature is good for un-doped  $\text{ZrSiO}_4$ . For assigning the modes, we assumed the mode assignment previously reported [29]. Since  $\text{Zr}_{0.95}\text{Ti}_{0.05}\text{SiO}_4$  and  $\text{ZrSiO}_4$  have similar Raman spectra (because they share the same crystal structure), the same mode assignment is assumed for both compounds. Notice that according to group theory, twelve Raman modes ( $\Gamma = 2A_{1g} + 4B_{1g} + B_{2g} + 5E_g$ ) are expected in the zircon structure [32]. However, usually only eight modes are measured in  $\text{ZrSiO}_4$  [31].

In the Raman spectrum of a zircon-type oxide, the high-frequency region ( $> 900\text{ cm}^{-1}$ ) corresponds to internal stretching vibrations of the  $\text{SiO}_4$  tetrahedron

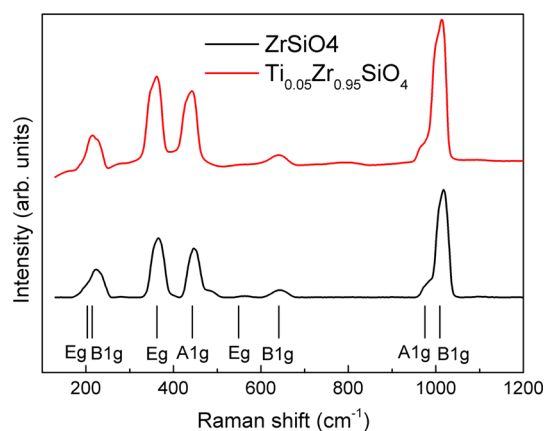


**Figure 4** Raman spectra of  $\text{Zr}_{0.95}\text{Ti}_{0.05}\text{SiO}_4$  (red line) and  $\text{ZrSiO}_4$  (black line) at ambient pressure. Ticks represent the position of Raman modes for zircon-type  $\text{ZrSiO}_4$  [31]. The mode assignment is shown.

**Table 1** Comparison of the Raman modes of zircon-type  $\text{ZrSiO}_4$  and  $\text{Ti}_{0.05}\text{Zr}_{0.95}\text{SiO}_4$  synthesized by the sol–gel method with the literature [31]

Mode	$\text{ZrSiO}_4$ [31]	$\text{ZrSiO}_4$	$\text{Ti}_{0.05}\text{Zr}_{0.95}\text{SiO}_4$
$E_g$	202.5(5)	203(1)	188(1)
$B_{1g}$	215.5(5)	223(1)	213(1)
$E_g$	357.5(5)	366(1)	361(1)
$A_{1g}$	439.5(5)	446(1)	441(1)
$E_g$	547.0(5)	562(1)	555(2)
$B_{1g}$	641.5(5)	642(1)	642(1)
$A_{1g}$	975.5(5)	976(1)	967(1)
$B_{1g}$	1009.0(5)	1018(1)	1015(1)

[33]. The intermediate-frequency region ( $540\text{--}650\text{ cm}^{-1}$ ) involves bending modes of the  $\text{SiO}_4$  tetrahedron [33] and the low-frequency modes are either external pure translations or rotations of the  $\text{SiO}_4$  molecule [33]. Therefore, it is not surprising the similitude between the Raman spectra of  $\text{Zr}_{0.95}\text{Ti}_{0.05}\text{SiO}_4$  and  $\text{ZrSiO}_4$ . The only difference (as seen in Table 1, the modes shift about  $10\text{ cm}^{-1}$ ) is the small decrease (less than 3%) in the frequencies of all modes in  $\text{Zr}_{0.95}\text{Ti}_{0.05}\text{SiO}_4$ . Therefore, the doping with titanium only promotes changes in the phonon frequencies, which is an indication that Ti has been incorporated into the structure of the doped sample substituting Zr [34]. However, Ti doping does not induce a breaking of symmetry selection rules. This should cause qualitative changes in the Raman spectrum [34], which are not the present case. The observed decrease in the Raman frequencies can be caused by weakening of the restoring forces as a consequence of subtle distortions of the coordination polyhedra [35]. A confirmation of this hypothesis requires further studies which are beyond the scope of this work; however, we think this is an indication that Ti has been incorporated into the structure of the doped sample substituting Zr.

Earlier reports observed the appearance of two peaks in the Raman spectrum when a low concentration of titanium is incorporated into silica glasses [3]. These modes were assigned to the presence of tetrahedrally coordinated titanium. Other authors attributed that tetrahedral Ti has its highest vibrational mode at  $700\text{--}800\text{ cm}^{-1}$  [4]. In more recent works, a consensus is reached that the formation of Ti–O–Si linkages is related to the appearance of a

peak in both Raman and infrared spectra at  $910\text{--}960\text{ cm}^{-1}$  [6]. No evidence of these modes was detected in our Ti-doped sample, being all the observed peaks consistent with a zircon-type structure. This fact could be interpreted as a confirmation that the 5% of  $\text{Ti}^{4+}$  (added during the synthesis) is incorporated into the tetragonal zircon structure of our  $\text{Zr}_{0.95}\text{Ti}_{0.05}\text{SiO}_4$  sample, taking Ti probably the Zr position in which it is coordinated by eight oxygen atoms.

### Hp-XRD

In Fig. 5, we show the XRD patterns of the  $\text{Zr}_{0.95}\text{Ti}_{0.05}\text{SiO}_4$  collected at different pressures. The main peaks of the tetragonal low-pressure phase of zircon ( $hkl = 101; 200; 211; 112$ ) are marked at the bottom of the figure with ticks, and dashed vertical lines are plotted up to guide the eye into the pressure-induced movement to higher  $2\theta$  positions of the (101) and (200) peaks.

In the XRD experiments, due to the angular opening of the DAC and the wavelength used, four peaks of the zircon structure were detected. We selected two non-equivalent peaks (the most intense) to determine the unit-cell parameters; the (200) peak was used to determine one lattice parameter ( $a$ ) and then, assuming this value, the (101) peak was used to determine the other lattice parameter ( $c$ ) [36]. No

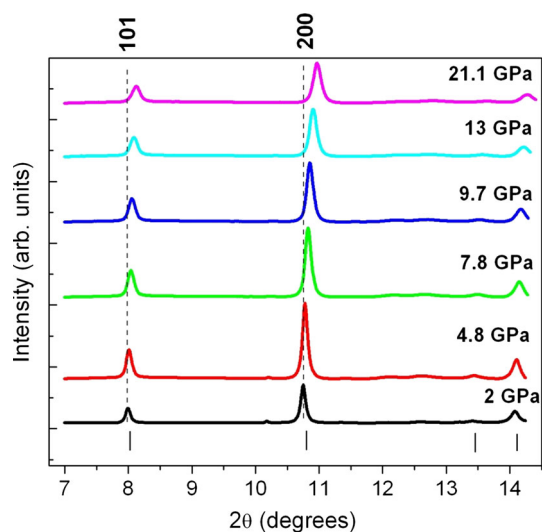


**Figure 5** HP-XRD patterns of  $\text{Zr}_{0.95}\text{Ti}_{0.05}\text{SiO}_4$  at selected pressures. Bragg peaks of the zircon structure are identified with ticks. Dashed lines facilitate the identification of the shift of (101) and (200) peaks.

evidence of any peaks corresponding to the high- or low-pressure phases of  $\text{ZrTiO}_4$  was observed within the accuracy of this method. The main peak [identified as (111)] of the low-pressure phase of  $\text{ZrTiO}_4$  should have been seen at  $2\theta \sim 12^\circ$  [37], but no indication of the presence of it could be observed in our experiments. On the other hand, no evidence of the transition to the scheelite-type [14] or monazite structure [38] is found in our experiments up to 21.1 GPa. Only beyond this pressure, the onset of the transition to a scheelite-type polymorph (known as reidite also) is found. In Fig. 6, we show the diffraction pattern taken at 31 GPa where the fingerprints of peaks of the scheelite-type (space group  $I4_1/a$ ) phase of  $\text{ZrSiO}_4$  [14] are noticed (see the arrows in the figure). In the pattern, the low-pressure (zircon) and high-pressure (scheelite) phases coexist. A determination of unit-cell volume of the low- and high-pressure phases at 31 GPa indicates a volume collapse of 10% associated to the phase transition. The present transition pressure (31 GPa) is larger than that of synthetic pure  $\text{ZrSiO}_4$  (19.7 GPa) and that of the natural zircon mineral, which has rare-earth impurities in a low concentration  $< 1\%$  and has an intermediate transition pressure of 23 GPa [14]. Thus, our and previous results support that the doping of  $\text{ZrSiO}_4$  enhances the structural stability, being the transition pressure higher for larger impurities concentration.

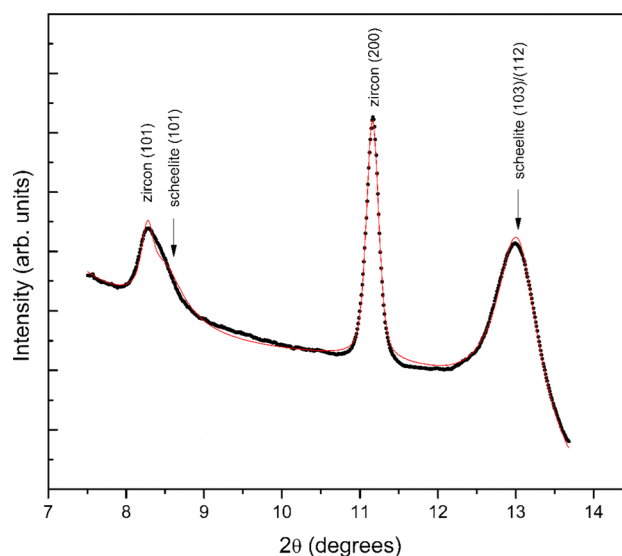


**Figure 6** HP-XRD pattern of  $\text{Zr}_{0.95}\text{Ti}_{0.05}\text{SiO}_4$  at 31 GPa. Arrows indicate the position of the Bragg peaks of the HP scheelite-type phase.

We will concentrate now on the compressibility of  $Zr_{0.95}Ti_{0.05}SiO_4$ . Since non-hydrostatic effects are known to influence the compressibility of zircon-type oxides [36], we will limit the analysis to the pressure range where the PTM can be considered as quasi-hydrostatic. In Fig. 7, we present the pressure dependence of the unit-cell parameters, which can be described by a linear function. The obtained linear compressibilities of  $Zr_{0.95}Ti_{0.05}SiO_4$  (which correspond to the red lines shown in the figure) are summarized in Table 2. The linear compressibilities of the  $a$  and  $c$  axes ( $K_a$  and  $K_c$ , respectively) are smaller than those reported for pure  $ZrSiO_4$  [12]. The fact that  $K_a/K_c$  is found to be 1.71 [12] for the pure sample, and 1.78 for the doped one (this work), suggests that, in the analyzed pressure range, the Ti incorporation into the zircon structure could have increased the crystal anisotropy during compression of  $Zr_{0.95}Ti_{0.05}SiO_4$ .

We will finally discuss the pressure dependence of the unit-cell volume. The results for the quasi-hydrostatic regime are represented in Fig. 8. We found

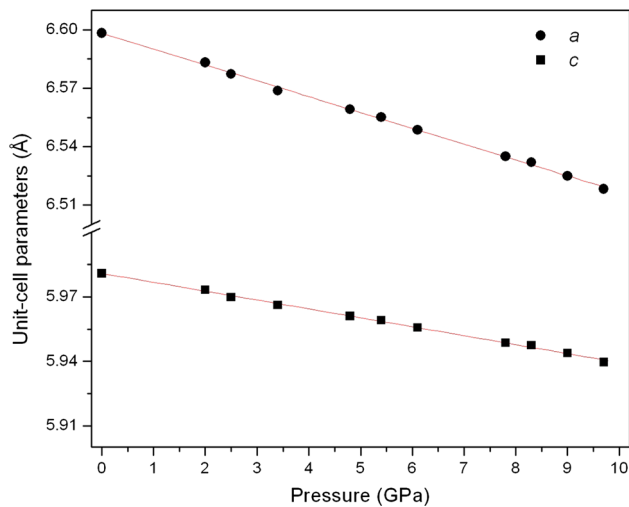


**Figure 7** Pressure dependence of the unit-cell parameters of  $Zr_{0.95}Ti_{0.05}SiO_4$  in the quasi-hydrostatic regime. Dots are the experimental data (included the ambient-pressure measurement), and the red lines represent the linear fits.

**Table 2** Linear compressibilities of  $K_a$  and  $K_c$  for  $Zr_{0.95}Ti_{0.05}SiO_4$  and  $ZrSiO_4$

Sample	$K_a$ ( $10^{-3} \text{ GPa}^{-1}$ )	$K_c$ ( $10^{-3} \text{ GPa}^{-1}$ )
Pure $ZrSiO_4$ [9]	1.68	0.98
$Zr_{0.95}Ti_{0.05}SiO_4$	1.23	0.69

that these results can be properly described by a third-order Birch–Murnaghan (BM3) equation of state (EoS) [39]. The fit is shown in the figure with a red line. From it, we determined for  $Zr_{0.95}Ti_{0.05}SiO_4$  its bulk modulus at ambient pressure  $B_0 = 297(5) \text{ GPa}$  and its pressure derivative  $B_0' = 2.8(6)$ , as well as the ambient-pressure volume  $V_0 = 260.4(7) \text{ \AA}^3$ . The bulk modulus is considerably larger (about a 30%) than the one found for pure  $ZrSiO_4$  [11, 14]. A comparison of the different  $B_0$  and  $B_0'$  can be seen in Table 3. The obtained results suggest that the incorporation of Ti reduces the compressibility of zircon. This conclusion is consistent with the theoretical predictions of a large bulk modulus (274.4 GPa) for zircon-type  $TiSiO_4$  [4, 5]. The one found here for  $Zr_{0.95}Ti_{0.05}SiO_4$  is even higher than calculated values for  $TiSiO_4$ , which makes  $Zr_{0.95}Ti_{0.05}SiO_4$  a potential candidate for super-hard material. The obtained large bulk modulus also rules out the possible incorporation of  $Ti^{4+}$  substituting Si instead of Zr which will imply a decrease in the bulk

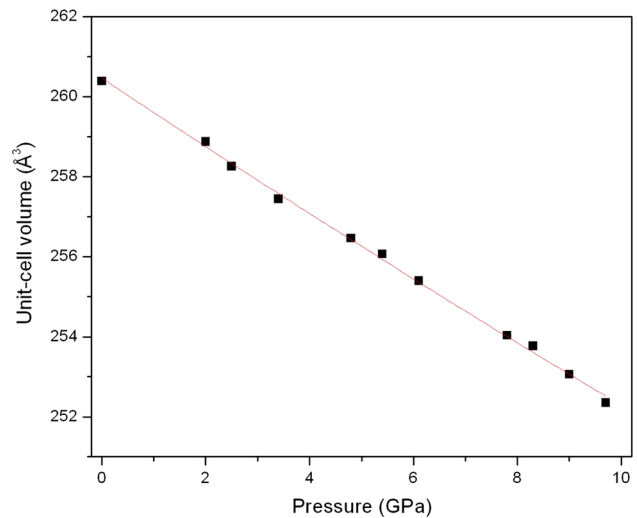


**Figure 8** Unit-cell volume (square dots) versus pressure for  $Zr_{0.95}Ti_{0.05}SiO_4$  and third-order Birch–Murnaghan EoS (solid line).

**Table 3** Bulk modulus and its pressure derivative of  $Zr_{0.95}Ti_{0.05}SiO_4$  compared with values previously reported for  $ZrSiO_4$  [11, 14]

Sample	$B_0$ (GPa)	$B_0'$ (dimensionless)
Pure $ZrSiO_4$ [11]	225(15)	6.5(1.6)
Pure $ZrSiO_4$ [14]	201(8)	3.1
$Zr_{0.95}Ti_{0.05}SiO_4$ (this work)	297(5)	2.8(6)

modulus because Ti–O bonds are more compressible than Si–O bonds [40]. Indeed, ZrTiO<sub>4</sub> is known to have a bulk modulus of 147 GPa [34].

## Conclusions

In this article, we have reported experimental evidence that the incorporation of Ti into the crystal structure of ZrSiO<sub>4</sub> induces a decrease in the compressibility and enhances the structural stability under compression. In particular, we have reported by the first time the synthesis and characterization of Zr<sub>0.95</sub>Ti<sub>0.05</sub>SiO<sub>4</sub>. The crystal structure (zircon-type) and Raman-active modes have been determined. In addition, we have studied the changes induced by pressure in the crystal structure. We found that the ambient-pressure phase remains stable below 31 GPa and that the HP phase is consistent with a scheelite-type structure. On the other hand, we studied the volumetric and axial compressibility of Zr<sub>0.95</sub>Ti<sub>0.05</sub>SiO<sub>4</sub> by means of high-pressure X-Ray diffraction using synchrotron radiation. The pressure dependence of the unit-cell volume has been analyzed using a third-order Birch–Murnaghan equation of state. The bulk modulus determined from the data collected under quasi-hydrostatic conditions ( $P < 10.1$  GPa) is 297 GPa, which is 30% greater than the one reported in the literature for pure zircon. This suggests that Zr<sub>0.95</sub>Ti<sub>0.05</sub>SiO<sub>4</sub> is a potential candidate for ultra-hard material.

## Acknowledgements

SEM and Raman measurements were performed at Y-TEC S. A. S. Ferrari, F. Grinblat and L. G. Pampillo thank the financial support provided by the Agencia Nacional de Promoción Científica y Tecnológica (ANPCyT) under Grant PICT-2012-1730. D. E. thanks the support of Spanish MINECO and European FEDER under Grant No. MAT2016-75586-C4-1-P. The authors thank the partial support from LNLS with Project XDS-18856.

## References

- [1] Grinblat F, Ferrari S, Pampillo LG, Saccone FD, Errandonea D, Santamaria-Perez D, Segura A, Vilaplana R, Popescu C (2017) Compressibility and structural behavior of pure and Fe-doped SnO<sub>2</sub> nanocrystals. *Solid State Sci* 64:91–98
- [2] Errandonea D, Ferrer-Roca C, Martinez-Garcia D et al (2010) High-pressure x-ray diffraction and ab initio study of Ni<sub>2</sub>Mo<sub>3</sub>N, Pd<sub>2</sub>Mo<sub>3</sub>N, Pt<sub>2</sub>Mo<sub>3</sub>N, Co<sub>3</sub>Mo<sub>3</sub>N, and Fe<sub>3</sub>Mo<sub>3</sub>N: two families of ultra-incompressible bimetallic interstitial nitrides. *Phys Rev B* 82:1–8
- [3] Rignanese GM, Rocquefelte X, Gonze X, Pasquarello A (2005) Titanium oxides and silicates as high- $\kappa$  dielectrics: a first-principles investigation. *Int J Quantum Chem* 101:793–801
- [4] Liu H, Liu ZT, Ren J et al (2017) Structural, electronic, mechanical, dielectric and optical properties of TiSiO<sub>4</sub>: first-principles study. *Solid State Commun* 251:43–49
- [5] Gracia L, Beltran A, Errandonea D (2009) Characterization of the TiSiO<sub>4</sub> structure and its pressure-induced phase transformations: density functional theory study. *Phys Rev B* 80:1–10
- [6] Seriani N, Pinilla C, Scandolo S (2017) Titania–silica mixed oxides investigated with density functional theory and molecular dynamics simulations. *Phys Status Solidi B* 254:11062–11067
- [7] Shwetha G, Kanchana V, Ramesh Babu K, Vaitheeswaran G, Valsakumar MC (2014) High-pressure structural stability and optical properties of scheelite-type ZrGeO<sub>4</sub> and HfGeO<sub>4</sub> X-ray phosphor hosts. *J Phys Chem C* 118:4325–4333
- [8] Page FZ, Fu B, Kita NT, Fournelle J, Spicuzza MJ, Schulze DJ, Viljoen F, Basei MAS, Valley JW (2007) Zircons from kimberlite: new insights from oxygen isotopes, trace elements, and Ti in zircon thermometry. *Geochim Cosmochim Acta* 71:3887–3903
- [9] Marqués M, Flórez M, Recio JM, Gerward L, Olsen JS (2006) Structure and stability of ZrSiO<sub>4</sub> under hydrostatic pressure. *Phys Rev B* 74:1–9
- [10] Tange Y, Takahashi E (2004) Stability of the high-pressure polymorph of zircon (ZrSiO<sub>4</sub>) in the deep mantle. *Phys Earth Planet Inter* 143–144:223–229
- [11] Scott HP, Williams Q, Knittle E (2002) Ultralow compressibility silicate without highly coordinated silicon. *Phys Rev Lett* 88:015506
- [12] Hazen RM, Finger LW (1979) Crystal structure and compressibility of zircon at high pressure. *Am Mineral* 64:196–201
- [13] Flórez M, Contreras-García J, Recio JM (2009) Quantum-mechanical calculations of zircon to scheelite transition pathways in ZrSiO<sub>4</sub>. *Phys Rev B* 79:1–11
- [14] van Westrenen W, Frank MR, Hanchar JM, Fei Y, Finch RJ, Zha C-S (2004) In situ determination of the compressibility of synthetic pure zircon (ZrSiO<sub>4</sub>) and the onset of the zircon-reidite phase transition. *Am Mineral* 89:197–203



- [15] Errandonea D, Kumar RS, Gracia L, Beltrán A, Achary SN, Tyagi AK (2009) Experimental and theoretical investigation of  $\text{ThGeO}_4$  at high pressure. *Phys Rev* 80:1–7
- [16] Manoun B, Downs RT, Saxena SK (2006) A high-pressure Raman spectroscopic study of hafnon,  $\text{HfSiO}_4$ . *Am Mineral* 91:1888–1892
- [17] Veytizou C, Quinson JF, Douy A (2000) Sol–gel synthesis via an aqueous semi-alkoxide route and characterization of zircon powders. *J Mater Chem* 10:365–370
- [18] Veytizou C, Quinson JF, Jorand Y (2002) Preparation of zircon bodies from amorphous precursor powder synthesized by sol–gel processing. *J Eur Ceram Soc* 22:2901–2909
- [19] Mao HK, Xu J, Bell PM (1986) Calibration of the Rubi Pressure Gauge to 800 kbar under quasi-hydrostatic conditions. *J Geophys Res* 91:4673–4676
- [20] Klotz S, Chervin JC, Munsch P, Le Marchand G (2009) Hydrostatic limits of 11 pressure transmitting media. *J Phys D* 4:1–8
- [21] Errandonea D, Muñoz A, Gonzalez-Platas J (2014) Comment on high-pressure x-ray diffraction study of  $\text{YBO}_3/\text{Eu}^{3+}$ ,  $\text{GdBO}_3$ , and  $\text{EuBO}_3$ : pressure-induced amorphization in  $\text{GdBO}_3$ . *J Appl Phys* 115:1–3
- [22] Errandonea D (2015) Exploring the properties of MTO<sub>4</sub> compounds using high-pressure powder x-ray diffraction. *Cryst Res Technol* 50:729–736
- [23] Lutterotti L, Bortolotti M, Ischia G, Lonardelli I, Wenk H-R (2007) Rietveld texture analysis from diffraction images. *Z Kristallogr* 26:125–130
- [24] Errandonea D, Kumar RS, Gomis O, Manjon FJ, Ursaki VV, Tiginyanu IM (2013) X-ray diffraction study on pressure-induced phase transformations and the equation of state of  $\text{ZnGa}_2\text{Te}_4$ . *J Appl Phys* 114:1–7
- [25] Tailby ND, Walker AM, Berry AJ et al (2011) Ti site occupancy in zircon. *Geochim Cosmochim Acta* 75(3):905–921
- [26] Popescu C, Sans JA, Errandonea D, Segura A, Villanueva R, Sapiña F (2014) Compressibility and structural stability of nanocrystalline  $\text{TiO}_2$  anatase synthesized from freeze-dried precursors. *Inorg Chem* 53:11598–11603
- [27] Heany PJ, Prewitt CT, Gibbs GV (1994) Silica: physical behaviour, geochemistry, and materials applications. Mineralogical Society of America, Washington, DC
- [28] Valigi M, Gazzoli D, Inccociati E, Dragone R (1997) Metastable phase formation in the  $\text{TiO}_2\text{–ZrO}_2$  and  $\text{CdO–ZrO}_2$  systems. *Solid State Ion* 101:597–603
- [29] Cappelletti G, Ardizzone S, Fermo P, Gilardoni S (2005) The influence of iron content on the promotion of the zircon structure and the optical properties of pink coral pigments. *J Eur Ceram Soc* 25:911–917
- [30] Ardizzone S, Binaghi L, Cappelletti G, Fermo P, Gilardoni S (2002) Iron doped zirconium silicate prepared by a sol-gel procedure. The effect of the reaction conditions on the structure, morphology and optical properties of the powders. *Phys Chem Chem Phys* 4:5683–5689
- [31] Syme RWG, Lockwood DJ, Kerr HJ (1977) Raman spectrum of synthetic zircon ( $\text{ZrSiO}_4$ ) and thorite ( $\text{ThSiO}_4$ ). *J Phys C* 10(8):1335–1348
- [32] Guedes I, Hirano Y, Grimsditch M, Wakabayashi N, Loong CK, Boatner LA (2001) Raman study of phonon modes in  $\text{ErVO}_4$  single crystals. *J Appl Phys* 90:1843–1846
- [33] Panchal V, Manjon FJ, Errandonea D, Rodríguez-Hernández P, Lopez-Solano J, Muñoz A, Achary SN, Tyagi AK (2011) High-pressure study of  $\text{ScVO}_4$  by Raman scattering and ab initio calculations. *Phys Rev B* 83:1–10
- [34] Mohaček-Grošev V, Vrankić M, Maksimović A, Mandić V (2017) Influence of titanium doping on the Raman spectra of nanocrystalline  $\text{ZnAl}_2\text{O}_4$ . *J Alloys Compd* 697:90–95
- [35] Panchal V, Errandonea D, Manjón FJ, Muñoz A, Rodríguez-Hernández P, Achary SN, Tyagi AK (2017) High-pressure lattice-dynamics of  $\text{NdVO}_4$ . *J Phys Chem Solids* 100:126–133
- [36] Garg AB, Errandonea D, Rodríguez-Hernández P, López-Moreno S, Muñoz A, Popescu C (2014) High-pressure structural behaviour of  $\text{HoVO}_4$ : combined XRD experiments and ab initio calculations. *J Phys: Condens Matter* 26:265402
- [37] Errandonea D et al (2010) New high-pressure phase of  $\text{HfTiO}_4$  and  $\text{ZrTiO}_4$  ceramics. *Mater Res Bull* 45:1732–1735
- [38] Lacomba-Perales R, Errandonea D, Meng Y, Bettinelli M (2010) High-pressure stability and compressibility of  $\text{APO}_4$  ( $A = \text{La, Nd, Eu, Gd, Er, and Y}$ ) orthophosphates: an x-ray diffraction study using synchrotron radiation. *Phys Rev* 81:1–9
- [39] Birch F (1952) Elasticity and constitution of the earth's interior. *J Geophys Res* 57:227–286
- [40] Ferry JM, Watson EB (2007) New thermodynamic models and revised calibrations for the Ti-in-zircon and Zr-in-rutile thermometers. *Contrib Mineral Petrol* 154:429–437